Multi-Chain Slip-Spring Simulations for Polyisoprene Melts

*Yuichi Masubuchi[1] and Takashi Uneyama[2]

[1] Department of Materials Physics,

[2] Center of Computational Science,

Nagoya University, Nagoya 4648603, JAPAN.

*To whom correspondence should be addressed

mas@mp.pse.nagoya-u.ac.jp

KEYWORDS

Molecular simulations; rheology; entanglement;

Submitted to Korea-Australia Rheology Journal on 28, June 2019

and published in vol. **31**, 2019, 241-248

ABSTRACT

The multi-chain slip-spring (MCSS) model is a coarse-grained molecular model developed for efficient simulations of the dynamics of entangled polymers. In this study, the simulations were examined for viscoelasticity of polyisoprene (PI) melts, for which the experimental data for well-characterized samples are available in the literature. The conversion factor for the molecular weight was determined from the fitting of the molecular weight dependence of zero-shear viscosity. According to the obtained value, linear viscoelasticity of several linear PI melts was calculated, and the units of time and modulus were determined. Based on the shift-factors reported experimentally for the time-temperature superposition, the conversion factors for time and modulus were obtained for different temperatures and used for the prediction of linear viscoelasticity of 6-arm star PI melts, and viscosity growth under high shear for linear PI melts. The predictions were in good agreement with the data, demonstrating the validity of the method. The conversion factors determined were consistent with those reported for polystyrene melt earlier, whereas the relations between the conversion factors are still unknown.

INTRODUCTION

The multi-chain slip-spring (MCSS) model is one of the coarse-grained multi-chain models for simulations of entangled polymers in molecular level (Masubuchi 2014; Masubuchi 2016a). Due to the slow relaxation nature, molecular dynamics simulations with atomistic details are practically difficult for entangled polymers, yet attempted (Baig et al. 2010b; Stephanou et al. 2010; Baig et al. 2010a). The widely used and established approach is the bead-spring type simulations (Kremer and Grest 1990). Recent studies with highly optimized computation codes have reported some simulation results for moderately entangled polymer melts, in which the bead number per chain was increased up to several hundred (Xu et al. 2015). For this approach, the computation costs are still high due to the inter-bead interaction, which is short-range and repulsive like the Lennard-Jones interaction. Such a short-range and strong repulsion limits the size of time step for the numerical integration rather small. In this respect, the simulations with softer interactions that allow interpenetration of the particles are favorable for the computation. However, the simulations with such softer interactions cannot reproduce the entangled polymer dynamics unless *ad-hoc* uncrossability between the chains is implemented (Pan and Manke 2003). Attempts have been made for realization of uncrossability via the inter-bond interaction (rather than the inter-bead interaction)(Kumar and Larson 2001) and via the geometrical consideration (Padding and Briels 2001). However, such rigorous

54 treatments for uncrossability demands computation comparable to calculations with the
55 conventional bead-spring simulations. An alternative approach is a slip-spring model, in
56 which the entanglement is replaced by a virtual spring that connects bead-spring chains
57 without short-range repulsive interactions. To mimic the entanglement, the anchoring
58 points of the virtual spring slide along the connected chains. The virtual spring is
59 annihilated by a certain probability when one of the anchoring points reaches the chain
60 end, and at each chain end, a new virtual spring is created to maintain the average number
61 of springs in the system. Although the computational efficiency is less than the multi-
62 chain slip-link model (Masubuchi et al. 2001; Masubuchi et al. 2004; Masubuchi 2016b)
63 owing to the soft interactions the simulations for moderately entangled systems are quite
64 efficient.

65 Inspired by the single-chain version (Likhtman 2005; Uneyama 2011), the multi-
66 chain slip-spring models have been developed by a few groups in parallel (Chappa et al.
67 2012; Uneyama and Masubuchi 2012; Langeloth et al. 2013; Ramírez-Hernández et al.
68 2013; Vogiatzis et al. 2017). The critical issue for multi-chain modeling is the inter-bead
69 interaction. For the single chain version, because one of the ends for the virtual spring is
70 anchored at a certain point in space and is not spatially coupled with other chains, the
71 conformational distribution of the chain reduces to that of an ideal chain when we

integrate-out the degrees of freedom for the anchoring points. This construction ensures that the ideal chain statistics is straightforwardly retained. In contrast, for the multi-chain models, because both ends of the virtual spring are connected to the mobile chains, the conformational distribution functions for the chains are affected by the inclusion of virtual springs. Indeed, they play a role as an attractive interaction between the segments to compress the chains. Because it has been established that the entanglement is purely kinetic and does not affect the chain statistics, this artificial effect of the virtual spring must be compensated. The rigorous treatment by the inter-bead repulsive, yet soft interaction has been proposed (Chappa et al. 2012; Uneyama and Masubuchi 2012), whereas the intermolecular interaction with a finite compressibility (Ramírez-Hernández et al. 2013) and the weak repulsive interaction employed in dissipative particle dynamics simulations (Langeloth et al. 2013; Masubuchi et al. 2016) are effective as well.

Nevertheless, the models with adequate treatments for the artifacts of the inclusion of virtual springs are capable to simulate a variety of polymeric systems including block-copolymers (Ramírez-Hernández et al. 2013; Ramírez-Hernández et al. 2018), mixtures of long and short chains (Langeloth et al. 2014), polymer solutions (Masubuchi et al. 2016), branch polymers (Masubuchi 2018), network polymers (Megariotis et al. 2018; Masubuchi and Uneyama 2019), etc. The simulations under fast

90 shear flows have also been attempted (Ramírez-Hernández et al. 2013; Masubuchi 2015;
91 Ramírez-Hernández et al. 2015; Masubuchi and Uneyama 2018a). The other important
92 direction is the linkage to the atomistic models (Sgouros et al. 2017; Vogiatzis et al. 2017)
93 and the other coarse-grained models (Masubuchi and Uneyama 2018b).

94 In this specific study, we shall report the consistency of the MCSS simulations
95 with the literature data for polyisoprene (PI) melts (Auhl et al. 2008; Matsumiya et al.
96 2014). In the earlier studies, we have evaluated the model by the comparison of
97 rheological data for polystyrene (PS) (Masubuchi 2018), and by the comparison to the
98 generic bead-spring model(Masubuchi and Uneyama 2018a; Masubuchi and Uneyama
99 2018c). Because the polymer dynamics is virtually universal and not strongly dependent
100 on the chemistry (Ferry 1980), the evaluation already performed would be sufficient.
101 However, parameter determination for specific chemistries is also necessary for practical
102 use. Besides, the parameters must be evaluated for the consistency to the other materials
103 and the theories. We have performed the MCSS simulations for several linear polymers
104 and a few star-branched polymers. For the linear polymers, the simulations under fast
105 shear flows were also conducted. We have confirmed that the simulation results are in
106 semi-quantitative agreement with the experimental data. The parameters used are
107 consistent with those for PS. Details are shown below.

MODEL AND SIMULATIONS

The MCSS model proposed earlier (Uneyama and Masubuchi 2012) is used with the modifications for shear flows (Masubuchi 2015) and the branch point dynamics (Masubuchi 2018). In this model, a number of Rouse chains are dispersed in a simulation box with a periodic boundary condition. The Rouse chains are connected by virtual springs, for which both ends hop between the Rouse beads along the chain. The virtual spring is annihilated with a certain probability when one of the ends comes to the chain end, and vice versa, new virtual springs are introduced at the chain ends.

The free energy is given by

$$\frac{F}{k_{\mathrm{B}}T} = \frac{3}{2b^2}\sum_{i,k}\left(\mathbf{R}_{i,k+1} - \mathbf{R}_{i,k}\right)^2 + \frac{3}{2N_s b^2}\sum_{\alpha}\left(\mathbf{R}_{S_{\alpha,1},S_{\alpha,2}} - \mathbf{R}_{S_{\alpha,3},S_{\alpha,4}}\right)^2 + e^{\nu/kT}\sum_{i,k,j,l}\exp\left[-\frac{3}{2N_s b^2}\left(\mathbf{R}_{i,k} - \mathbf{R}_{j,l}\right)^2\right] \quad (1)$$

The first and second terms in the right-hand side are the contributions from the Rouse springs and the virtual springs, respectively. b is the average bond length between the Rouse segments, $\mathbf{R}_{i,k}$ is the position of the Rouse beads k on the chain i, and N_s is the parameter that determines the intensity of the virtual spring. $S_{\alpha,j}$ is the connectivity matrix for the virtual spring α. The third term is the soft-core repulsive interaction between the Rouse beads to eliminate the artificial effect on the chain statistics from the

126 virtual springs. $e^{\nu/kT}$ is the activity of the virtual springs to control the density of virtual
127 springs in the system by a grand canonical manner according to the chemical potential ν.
128 The governing equations and algorithms for the dynamics were derived from the
129 total free energy of the system to fulfill the detailed balance. The time development of
130 $\mathbf{R}_{i,k}$ obeys the Langevin equation of motion, and the SLLOD method was implemented
131 for the application of shear flows (Masubuchi 2015). The Glauber dynamics manage the
132 hopping of the virtual springs. For the branch polymers, the hopping across the branch
133 point (the so-called SHAB) is also considered, yet such a mechanism is not essential for
134 symmetric star polymers (Masubuchi 2018). The annihilation and creation of the virtual
135 springs are in balance under equilibrium by the master equation. For these dynamical
136 equations, in addition to the parameters that appear in the free-energy ($e^{\nu/kT}$ and N_{s}),
137 the friction coefficient for the bead motion ζ and that for the kinetics of virtual spring
138 ζ_{s} are introduced. For simplicity, we assume $\zeta = \zeta_{\mathrm{s}}$. See the previous publication for
139 further details, the numerical implementation (Uneyama and Masubuchi 2012).
140 Simulations were performed for linear, and star-branched polymer melts with
141 dimensionless units, for which the units of length, energy, and time are the bond length
142 b, the thermal energy $k_{\mathrm{B}}T$, and the diffusion time of a single bead $\tau_0 \equiv \zeta b^2/k_{\mathrm{B}}T$. For
143 convenience, to compare the simulated results with experimental data, we employ the unit

144 of molecular weight (i.e., corresponding molecular weight for the single bead) M_0 and
145 the unit of modulus $G_0 \sim b^3/k_\mathrm{B}T$, instead of the units of length and energy. For each case,
146 200 molecules are placed in the simulation box. Owing to the previous studies, $e^{\nu/kT}$
147 and N_s were fixed at 0.036 and 0.5, respectively. The bead number density ρ_b was 4.
148 These values attain a particular density of slip-springs, which are distributed along the
149 chain with the average number of Rouse beads between consecutive anchoring points of
150 slip-springs, $N_\mathrm{e}^{\mathrm{SS}} = 3.5$.

151 Periodic boundary conditions were employed with the Lees-Edwards boundary
152 under shear. The systems were sufficiently equilibrated before data acquisition. The linear
153 relaxation modulus $G(t)$ was calculated from the stress auto-correlation obtained from
154 equilibrium simulations for an extended period that is at least ten times larger than the
155 longest relaxation time. From $G(t)$, storage and loss moduli, $G'(\omega)$ and $G"(\omega)$, were
156 obtained by the fitting of $G(t)$ to a multi-mode Maxwell function. The zero-shear
157 viscosity η_0 was obtained from $G(t)$. For statistics, eight independent simulation runs
158 starting from different initial configurations were performed for each condition, and the
159 results reported below are the averaged values.

160

161 RESULTS

Figure 1 shows the molecular weight M dependence of η_0 for linear polymers in comparison to the data for PI melts reported experimentally (Gotro and Graessley 1984; Abdel-Goad et al. 2004; Auhl et al. 2008). The simulation result indicated by the solid red curve reasonably captures the data, including the onset of entanglement. Namely, the viscosity increases with an increase of M with a power-law manner, for which the exponent is unity in the low-M regime, whereas it is around 3.5 in the high-M regime. The transition between unentangled to entangled regimes is shown in a further clarity in the bottom panel, in which the viscosity is reduced by M^3, which is the scaling prediction given by the classical tube model (Doi and Edwards 1986). Indeed, the critical molecular weight for the onset of entanglement is indicated by the minimum of η_0/M^3. From this comparison, the conversion factor for the molecular weight of PI melt is determined as $M_0 = 400$ (g/mol).

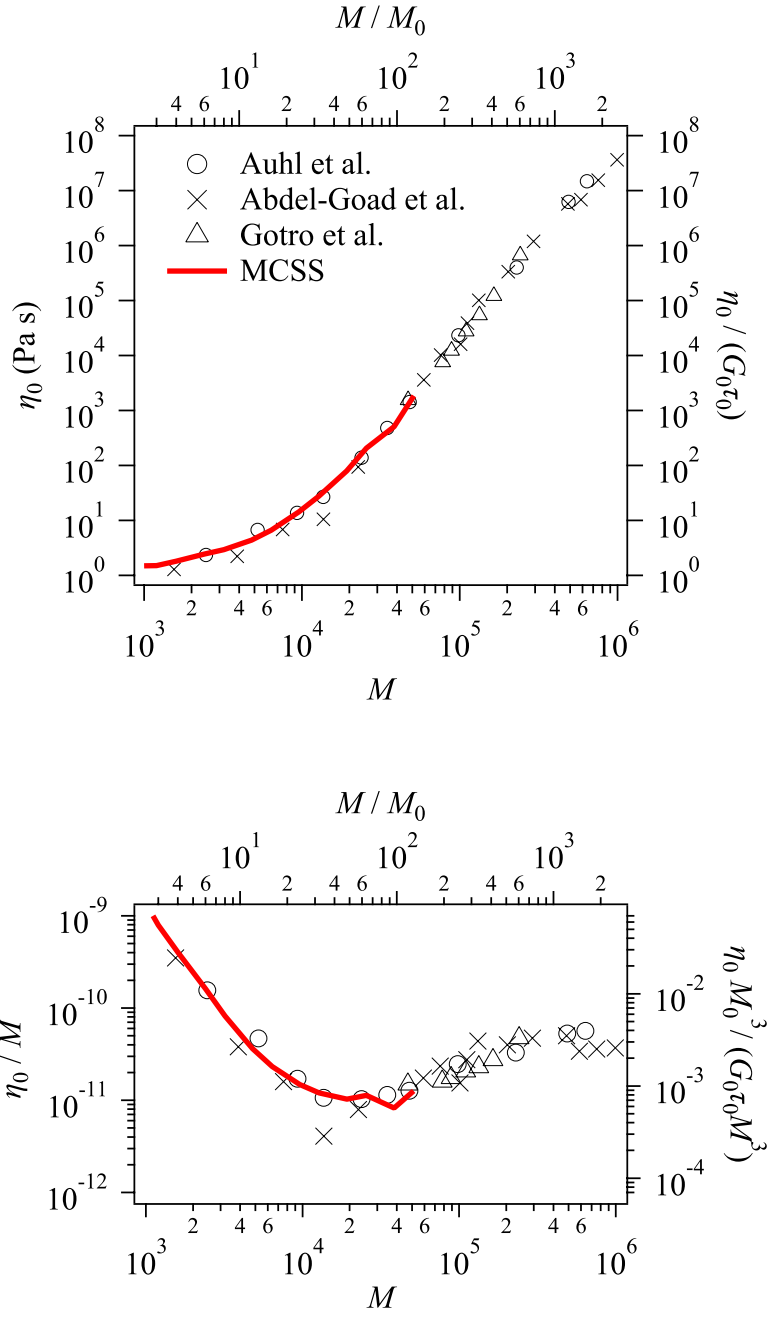

Figure 1 Molecular weight dependence of zero-shear viscosity for linear polymers (top) and the viscosity normalized by the classical reptation prediction (bottom). The data for PI melts at 25℃ (Gotro and Graessley 1984; Abdel-Goad et al. 2004; Auhl et al. 2008) are shown for comparison by symbols, and the simulation result is indicated by the solid curve.

Figure 2 shows the linear viscoelastic response for linear and star polymers. The

literature data of PI melts (Auhl et al. 2008; Matsumiya et al. 2014) are shown for comparison for the samples that have the molecular weights comparable to the simulated chains according to the conversion factor M_0 obtained above. For linear PI (seen in the top panel), the conversion factors for time and modulus are chosen as $\tau_0 = 5 \times 10^{-7}$sec and $G_0 = 2 \times 10^6$Pa at 25℃. These values give the unit viscosity $\tau_0 G_0 = 1$ Pa s, which is consistent with the result shown in Figure 1. With the same set of the conversion factors, the data for several different molecular weights are reasonably reproduced, except the high-ω behavior for the shortest chain, due to an unavoidable cut-off of the model.

For branch polymers, the conversion factors must be shared with those for linear polymers. Because the experimental data for star PI employed here (Matsumiya et al. 2014) were taken at 40℃, which is different from that for the linear polymers, we utilized the shift factors for PI melts reported experimentally (Auhl et al. 2008) to obtain the conversion factors. The determined values are $\tau_0 = 1.5 \times 10^{-6}$ sec and $G_0 = 2.1 \times 10^6$ Pa (at 40℃), and the comparison based on the conversion is shown in the bottom panel. The prediction is not excellent, although it works to some extent. We wish to note that better reproducibility has been reported for linear and branch polystyrenes (Masubuchi 2018), for which the reference temperature is identical and the data are reported from the same group.

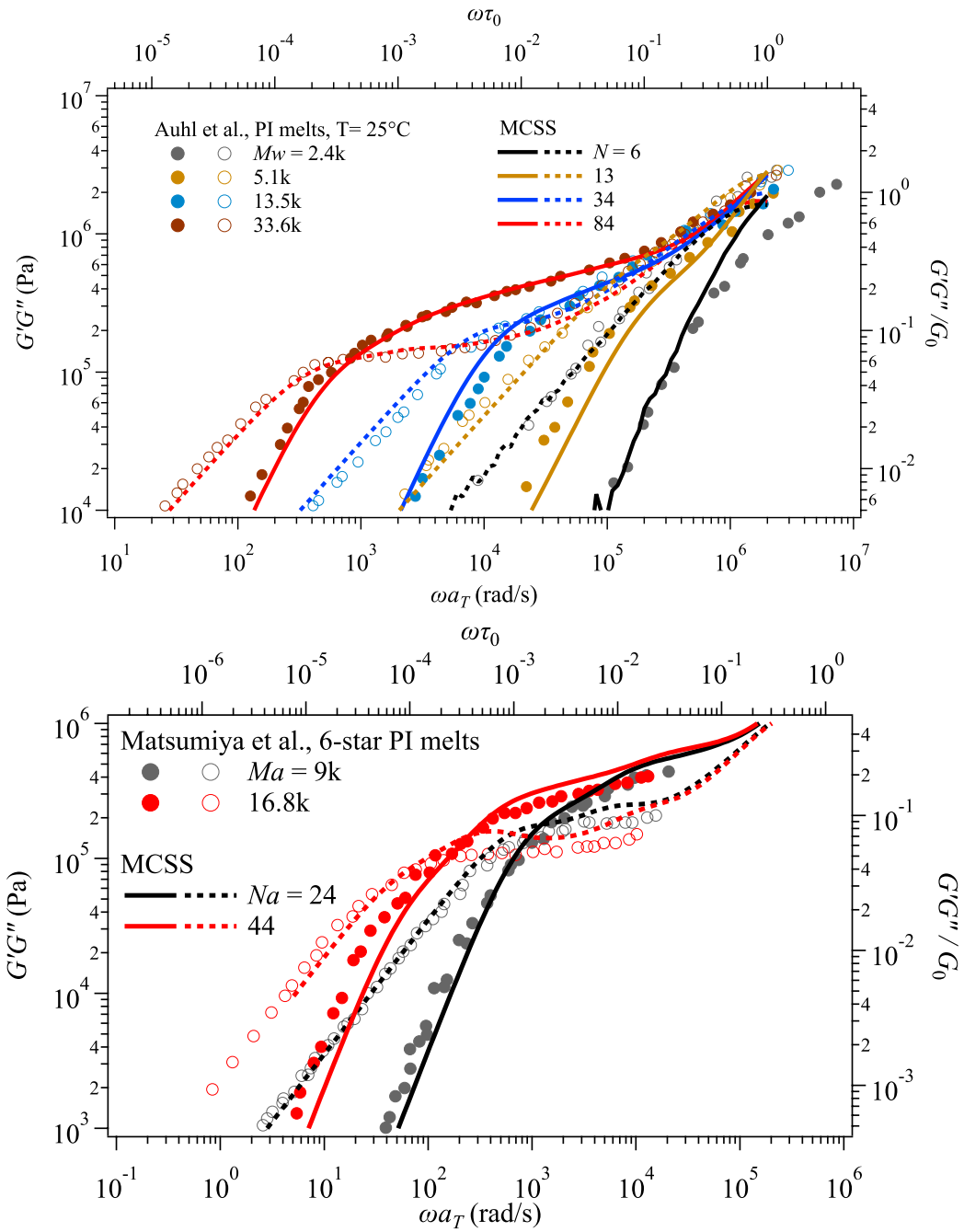

200

201

202 **Figure 2** Linear viscoelasticity of linear (top) and 6-arm star-branched (bottom) polymer
203 melts compared to the experimental data for PI with corresponding molecular weights
204 indicated in the figures (Auhl et al. 2008; Matsumiya et al. 2014). For the star polymers,
205 the molecular weight and the bead number of each arm are indicated. The experimental
206 data were taken at 25°C for linear PI and 40°C for star PI, respectively.

207

208 Figure 3 shows the viscosity growth for a few linear polymers, for which the

linear viscoelasticity is shown in Figure 2. For the prediction of nonlinear viscoelasticity, the conversion factors must be shared with those for linear viscoelasticity. We accommodated the temperature difference employing the shift factors reported (Auhl et al. 2008) and obtained the conversion factors at -35℃ as $\tau_0 = 2.8 \times 10^{-3}$sec and $G_0 = 1.7 \times 10^6$Pa. The simulation results according to these conversion factors are in excellent agreement for the short PI (Mw =13.5k shown in the top panel), whereas the simulations are not entirely consistent with the data for the long PI (Mw =33.6k shown in the bottom panel). In particular, the predictions for high shear rates are underestimated. This inconsistency might be due to the model construction, in which we assume that the system is not far from equilibrium. Meanwhile, we wish to note that the MCSS prediction under high shear is in good agreement with the results obtained from the bead-spring simulations (Masubuchi and Uneyama 2018c). Note also that better agreement can be attained if the conversion factors could be tuned.

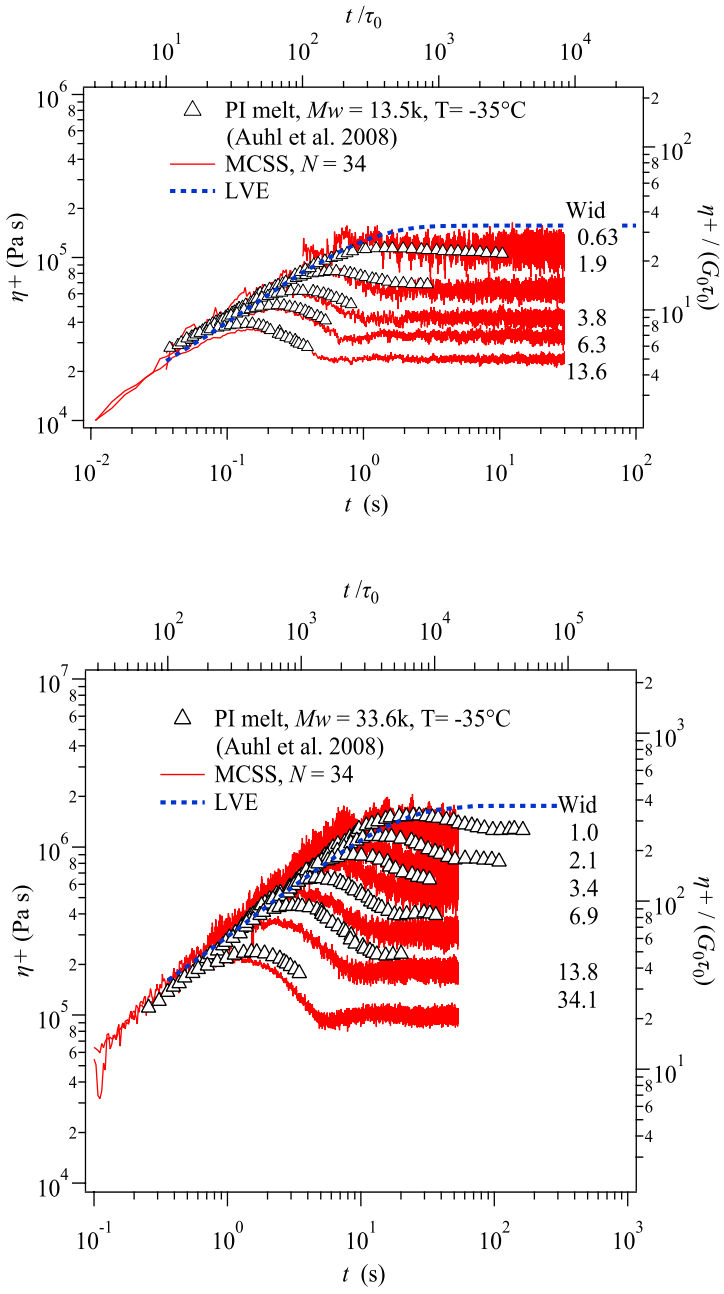

Figure 3 Viscosity growth under high shear for linear polymers compared with the experimental data for PI melts taken at -35℃ (Auhl et al. 2008). The bead number per chain and the corresponding molecular weight of PI are $N = 34$ and Mw =13.5k (top), and $N = 84$ and Mw =33.6k (bottom). The simulation results and the experimental data are shown by the red curve and triangle, respectively. The linear viscoelastic envelope is shown by the blue dotted curve. The shear rate is indicated in terms of the Weissenberg number for the longest relaxation time.

DISCUSSION

Let us discuss the unit of molecular weight M_0, which has been determined as 400 for PI in this study. This value is consistent with the previous study for PS, for which $M_0 = 1250$ (Masubuchi 2018) if we consider the entanglement molecular weight. Because M_0 is the molecular weight being carried by the single bead, and $N_e^{SS} = 3.5$, the molecular weight between two anchoring points of slip-springs M_e^{SS} is 1400 for PI and 4375 for PS. Both of these values are around four times smaller than the tabulated values for the entanglement molecular weight M_e. For instance, M_e values for PI and PS have been reported as 4820 (Auhl et al. 2008) and 14470 (Likhtman and McLeish 2002) based on the tube model. One of the reasons for the difference between M_e^{SS} and M_e is the model dependence of the relation between the plateau modulus and the density of entanglement. As we have discussed in the previous publications (Masubuchi et al. 2003; Masubuchi and Uneyama 2018b), the relation between the plateau modulus and the number density of entanglements is model dependent as written by $G_N = Ank_BT$. Here, A is the model-dependent factor that depends on the fluctuations considered, and n is the number density of entanglement segments. For most of the cases, the value of M_e experimentally reported is obtained for $A = 1$, which is for the affine network theory

without any fluctuation at entanglement. Meanwhile, $A = 0.8$ for the tube model due to the chain sliding at the entanglement, and $A = 0.5$ for the cross-link network models with Brownian motion of the entanglement. We have reported that our MCSS simulation gives $A = 0.17$, which seems reasonable because of the various fluctuations including the chain sliding (i.e., the hopping of the slip-spring, which causes the fluctuation of numbers of beads between entanglements), and the Brownian motion of the beads and the conformational fluctuations of the slip-spring (which causes the fluctuation of transient link positions) (Masubuchi and Uneyama 2018b). Based on $A = 0.17$, $M_{\mathrm{e}}^{\mathrm{SS}}$ can be calculated from M_{e} mentioned above as 1024 and 3074 for PI and PS, respectively. These values are even smaller than the $M_{\mathrm{e}}^{\mathrm{SS}}$ determined from the fitting, possibly due to the difference of the segment density.

The unit of modulus G_0 obtained for PI is also consistent with that obtained for PS earlier (Masubuchi 2018). For PI, $G_0 = 2 \times 10^6 \mathrm{Pa}$ (at 25℃), whereas for PS, $G_0 = 9.1 \times 10^5 \mathrm{Pa}$ (at 169.5℃). Both of these values are around three times larger than the plateau modulus reported, implying the consistency between the simulations for PI and PS. However, the relation between G_0 and M_0 seems non-trivial. From dimensional analysis, we obtain a relationship $G_0 = B\rho RT/M_0$. Here, B is a constant, ρ is the density, and R is the gas constant. Note that this relation is similar to, yet different from

that discussed above for G_N and M_e. For the tube model proposed by Likhtman and McLeish (Likhtman and McLeish 2002), it has been reported that ${M_0}^{\mathrm{LM}} = 4820$ and ${G_0}^{\mathrm{LM}} = 6 \times 10^5\,\mathrm{Pa}$ for the PI melt examined in this study. With the density of $\rho = 0.913\,\mathrm{g/cm^3}$, these values give $B^{\mathrm{LM}} = 1.3$. For our case, $B = 0.35$. We have no explanation for this value of B.

Let us turn our attention to the unit of time that was determined as $\tau_0 = 5 \times 10^{-7}$sec. According to the study by Auhl et al.(Auhl et al. 2008), the values for the tube model are ${\tau_0}^{\mathrm{LM}} = 1.3 \times 10^{-5}$. The difference for the unit of time can be explained by the unit of molecular weight. For the tube model, ${M_0}^{\mathrm{LM}} = 4820$ has been reported, whereas our simulation gives $M_0 = 400$. Because the unit of time corresponds to the Rouse relaxation time of the segment, the ratio for the unit of time would be the square of the ratio for the unit of molecular weight. This estimation is consistent with the values mentioned above. Similar consistency with the tube model can be confirmed for PS.

It is fair to note that Ramírez-Hernández et al.(Ramírez-Hernández et al. 2015) have reported a similar simulation study for the rheology of linear PI melts examined above. Their model, so-called TIEPOS (theoretically informed entangled polymer simulations), is the same with our MCSS model in the fundamental construction, in which bead-spring chains with weakly repulsive interactions are connected by virtual springs.

The main difference is that they consider the inter-bead interaction based on the compressibility, whereas we introduce the interaction to retain the ideal chain statistics. The other difference is that they allow only one slip-spring connected to a single bead to avoid passing between slip-springs along the chain. Probably due to these differences, the effect of slip-spring on the chain dynamics seems not the same with each other. To reproduce the viscoelasticity of PI melt with Mw =33.6k, we need the bead number per chain of $N = 84$, whereas they only have $N = 32$. The average number of slip-springs on one chain Z is 25 for our case, whereas 8.6 for them. This comparison demonstrates that their model has an advantage in the level of coarse-graining and for a reduction of computation costs. However, the efficiency of their entanglement is inexplicable from the discussion for $M_{\mathrm{e}}^{\mathrm{SS}}$ mentioned above. According to the difference of Z, a naïve estimation of A value for TIEPOS would be ca. 0.5, which is close to the cross-link networks. This estimation implies that the incompressibility for the chains, and the uncrossability between slip-springs significantly suppress the fluctuations around their entanglement. Besides, they compared the statistical distributions of their model with predictions by a mean-field single-chain model, and reported that the simulation data agree well with the theoretical predictions. Their result implies that the fluctuations in TIEPOS model is close to those in the mean-field single-chain model. However, in multi-

chain models, in general, the environment around a chain fluctuates (because the environment itself consists of fluctuating chains) and the statistical distributions deviate from the mean-field statistics without fluctuations. The friction for the slip-spring kinetics is the other important parameter, but the setting in TIEPOS seems the same with our simulations. Nevertheless, further assessment is necessary for the nature of the multi-chain slip-spring models.

CONCLUSIONS

We performed MCSS simulations with the model parameters fixed at $e^{\nu/kT} = 0.036$, $N_s = 0.5$, $\zeta = \zeta_s$, and $\rho_b = 4$ to compare the results with the experimental data for PI melts. The conversion factor for the molecular weight (i.e., the molecular weight carried by the single Rouse bead) was obtained as $M_0 = 400$ (g/mol) from the molecular weight dependence of the zero-shear viscosity for linear polymers. According to the M_0 value, we calculated the linear viscoelasticity for several linear and 6-arm star-branch polymers, for which the experimental data are available for PI with the corresponding molecular weight. For the linear polymers, the simulation results agree with the data for the conversion factors obtained by the fitting as $\tau_0 = 5 \times 10^{-7}$sec and $G_0 = 2 \times 10^6$Pa at 25℃. Based on these values, the conversion factors for different temperatures were

obtained according to the shift factors reported experimentally. With these conversion factors, the simulation results for linear viscoelasticity of star PI taken at 40℃, and for viscosity growth under high shear of linear PI obtained at -35℃ are in reasonable agreement with the experimental data. The conversion factors thus determined are consistent with those for PS. However, the relations between the conversion factors are still unknown, and further evaluation and systematic studies are necessary. For example, the dependence of conversion factors on the model parameters is worth investigating. Studies in such directions are ongoing, and the results will be published elsewhere.

Acknowledgments

This study was supported in part by Grant-in-Aid for Scientific Research (A) (17H01152), (B)(19H01861) and for Scientific Research on Innovative Areas (18H04483) from JSPS.

REFERENCES

Abdel-Goad M, Pyckhout-Hintzen W, Kahle S, Allgaier JJ, Richter D, Fetters LJ (2004) Rheological Properties of 1,4-Polyisoprene over a Large Molecular Weight Range. Macromolecules 37:8135–8144 . doi: 10.1021/ma030557+

Auhl D, Ramirez J, Likhtman AE, Chambon P, Fernyhough C (2008) Linear and

nonlinear shear flow behavior of monodisperse polyisoprene melts with a large range of molecular weights. J Rheol (N Y N Y) 52:801–835 . doi: 10.1122/1.2890780

Baig C, Mavrantzas VG, Kröger M (2010a) Flow Effects on Melt Structure and Entanglement Network of Linear Polymers: Results from a Nonequilibrium Molecular Dynamics Simulation Study of a Polyethylene Melt in Steady Shear. Macromolecules 43:6886–6902 . doi: 10.1021/ma100826u

Baig C, Stephanou PS, Tsolou G, Mavrantzas VG, Kröger M, Kroeger M, Kr??ger M, Kroeger M (2010b) Understanding Dynamics in Binary Mixtures of Entangled cis-1, 4-Polybutadiene Melts at the Level of Primitive Path Segments by Mapping Atomistic Simulation Data onto the Tube Model. Macromolecules 43:8239–8250 . doi: 10.1021/ma101211b

Chappa VC, Morse DC, Zippelius A, Müller M (2012) Translationally Invariant Slip-Spring Model for Entangled Polymer Dynamics. Phys Rev Lett 109:148302 . doi: 10.1103/PhysRevLett.109.148302

Doi M, Edwards SF (1986) The Theory of Polymer Dynamics. Clarendon press, Oxford

Ferry JD (1980) Viscoelastic Properties of Polymers, 3rd edn. John Wiley & Sons, Inc.

Gotro JT, Graessley WW (1984) Model hydrocarbon polymers: rheological properties

359 of linear polyisoprenes and hydrogenated polyisoprenes. Macromolecules
360 17:2767–2775 . doi: 10.1021/ma00142a058
361 Kremer K, Grest GS (1990) Dynamics of entangled linear polymer melts: A molecular-
362 dynamics simulation. J Chem Phys 92:5057 . doi: 10.1063/1.458541
363 Kumar S, Larson RG (2001) Brownian dynamics simulations of flexible polymers with
364 spring–spring repulsions. J Chem Phys 114:6937 . doi: 10.1063/1.1358860
365 Langeloth M, Masubuchi Y, Böhm MC, Müller-plathe F (2013) Recovering the
366 reptation dynamics of polymer melts in dissipative particle dynamics simulations
367 via slip-springs. J Chem Phys 138:104907 . doi: 10.1063/1.4794156
368 Langeloth M, Masubuchi Y, Böhm MC, Müller-Plathe F (2014) Reptation and
369 constraint release dynamics in bidisperse polymer melts. J Chem Phys
370 141:194904 . doi: 10.1063/1.4901425
371 Likhtman AE (2005) Single-chain slip-link model of entangled polymers: simultaneous
372 description of neutron spin-echo, rheology, and diffusion. Macromolecules
373 38:6128–6139 . doi: 10.1021/ma050399h
374 Likhtman AE, McLeish TCB (2002) Quantitative theory for linear dynamics of linear
375 entangled polymers. Macromolecules 35:6332–6343 . doi: 10.1021/ma0200219
376 Masubuchi Y (2016a) Molecular Modeling for Polymer Rheology. In: Reference

377 Module in Materials Science and Materials Engineering. Elsevier, pp 1–7
378 Masubuchi Y (2014) Simulating the Flow of Entangled Polymers. Annu Rev Chem
379 Biomol Eng 5:11–33 . doi: 10.1146/annurev-chembioeng-060713-040401
380 Masubuchi Y (2016b) PASTA and NAPLES: Rheology Simulator. In: Computer
381 Simulation of Polymeric Materials. Springer Singapore, Singapore, pp 101–127
382 Masubuchi Y (2018) Multichain Slip-Spring Simulations for Branch Polymers.
383 Macromolecules 51:10184–10193 . doi: 10.1021/acs.macromol.8b01739
384 Masubuchi Y (2015) Effects of degree of freedom below entanglement segment on
385 relaxation of polymer configuration under fast shear in multi-chain slip-spring
386 simulations. J Chem Phys 143:224905 . doi: 10.1063/1.4937172
387 Masubuchi Y, Ianniruberto G, Greco F, Marrucci G (2004) Molecular simulations of the
388 long-time behaviour of entangled polymeric liquids by the primitive chain network
389 model. Model Simul Mater Sci Eng 12:S91–S100 . doi: 10.1088/0965-
390 0393/12/3/S03
391 Masubuchi Y, Ianniruberto G, Greco F, Marrucci G (2003) Entanglement molecular
392 weight and frequency response of sliplink networks. J Chem Phys 119:6925–
393 6930 . doi: 10.1063/1.1605382
394 Masubuchi Y, Langeloth M, Böhm MC, Inoue T, Müller-Plathe F (2016) A Multichain

395 Slip-Spring Dissipative Particle Dynamics Simulation Method for Entangled
396 Polymer Solutions. Macromolecules 49: . doi: 10.1021/acs.macromol.6b01971
397 Masubuchi Y, Takimoto J-I, Koyama K, Ianniruberto G, Marrucci G, Greco F (2001)
398 Brownian simulations of a network of reptating primitive chains. J Chem Phys
399 115:4387 . doi: 10.1063/1.1389858
400 Masubuchi Y, Uneyama T (2019) Retardation of the reaction kinetics of polymers due
401 to entanglement in the post-gel stage in multi-chain slip-spring simulations. Soft
402 Matter. doi: 10.1039/C9SM00681H
403 Masubuchi Y, Uneyama T (2018a) Comparison among multi-chain models for
404 entangled polymer dynamics. Soft Matter 14:5986–5994 . doi:
405 10.1039/C8SM00948A
406 Masubuchi Y, Uneyama T (2018b) Comparison among multi-chain models for
407 entangled polymer dynamics. Soft Matter 14:5986–5994 . doi:
408 10.1039/c8sm00948a
409 Masubuchi Y, Uneyama T (2018c) Comparison among Multi-Chain Simulations for
410 Entangled Polymers under Fast Shear. ECS Trans 88:161–167 . doi:
411 10.1149/08801.0161ecst
412 Matsumiya Y, Masubuchi Y, Inoue T, Urakawa O, Liu C-Y, van Ruymbeke E,

413 Watanabe H (2014) Dielectric and Viscoelastic Behavior of Star-Branched
414 Polyisoprene: Two Coarse-Grained Length Scales in Dynamic Tube Dilation.
415 Macromolecules 47:7637–7652 . doi: 10.1021/ma501561y
416 Megariotis G, Vogiatzis GG, Sgouros AP, Theodorou DN (2018) Slip spring-based
417 mesoscopic simulations of polymer networks: Methodology and the corresponding
418 computational code. Polymers (Basel) 10: . doi: 10.3390/polym10101156
419 Padding JT, Briels WJ (2001) Uncrossability constraints in mesoscopic polymer melt
420 simulations: Non-Rouse behavior of C[sub 120]H[sub 242]. J Chem Phys
421 115:2846 . doi: 10.1063/1.1385162
422 Pan G, Manke CW (2003) Developments Toward Simulation of Entangled Polymer
423 Melts By Dissipative Particle Dynamics (Dpd). Int J Mod Phys B 17:231–235 .
424 doi: 10.1142/S0217979203017400
425 Ramírez-Hernández A, Detcheverry FA, Peters BL, Chappa VC, Schweizer KS, Müller
426 M, de Pablo JJ (2013) Dynamical Simulations of Coarse Grain Polymeric Systems:
427 Rouse and Entangled Dynamics. Macromolecules 46:6287–6299 . doi:
428 10.1021/ma400526v
429 Ramírez-Hernández A, Peters BL, Andreev M, Schieber JD, de Pablo JJ (2015) A
430 multichain polymer slip-spring model with fluctuating number of entanglements

for linear and nonlinear rheology. J Chem Phys 143:243147 . doi: 10.1063/1.4936878

Ramírez-Hernández A, Peters BL, Schneider L, Andreev M, Schieber JD, Müller M, Kröger M, De Pablo JJ (2018) A detailed examination of the topological constraints of lamellae-forming block copolymers. Macromolecules 51:2110–2124 . doi: 10.1021/acs.macromol.7b01485

Sgouros AP, Megariotis G, Theodorou DN (2017) Slip-Spring Model for the Linear and Nonlinear Viscoelastic Properties of Molten Polyethylene Derived from Atomistic Simulations. Macromolecules 50:4524–4541 . doi: 10.1021/acs.macromol.7b00694

Stephanou PS, Baig C, Tsolou G, Mavrantzas VG, Kröger M, Kroeger M, Kröger M, Kröger M (2010) Quantifying chain reptation in entangled polymer melts: Topological and dynamical mapping of atomistic simulation results onto the tube model. J Chem Phys 132:124904 . doi: 10.1063/1.3361674

Uneyama T (2011) Single Chain Slip-Spring Model for Fast Rheology Simulations of Entangled Polymers on GPU. Nihon Reoroji Gakkaishi 39:135–152 . doi: 10.1678/rheology.39.135

Uneyama T, Masubuchi Y (2012) Multi-chain slip-spring model for entangled polymer dynamics. J Chem Phys 137:154902 . doi: 10.1063/1.4758320

Vogiatzis GG, Megariotis G, Theodorou DN (2017) Equation of State Based Slip Spring Model for Entangled Polymer Dynamics. Macromolecules 50:3004–3029 . doi: 10.1021/acs.macromol.6b01705

Xu X, Chen J, An L (2015) Simulation studies on architecture dependence of unentangled polymer melts. J Chem Phys 142:074903 . doi: 10.1063/1.4908262